AMOC as the key driver of the spread in Mid-Holocene winter temperature patterns over Europe in PMIP3 models

Alina Găinuşă-Bogdan, Didier Swingedouw, Pascal Yiou, Julien Cattiaux, Francis Codron

AMOC as the key driver of the spread in Mid-Holocene winter temperature patterns over Europe in PMIP3 models

Alina Găinuşă-Bogdan[1,2], Didier Swingedouw[1], Pascal Yiou[2], Julien Cattiaux[3] and Francis Codron[4]

[1] *Environnements et Paléoenvironnements Océaniques et Continentaux (EPOC), UMR CNRS 5805 EPOC—OASU—Université de Bordeaux, Allée Geoffroy Saint-Hilaire, Pessac 33615, France.*

[2] *Laboratoire des Sciences du Climat et de l'Environnement, UMR8212 CEA-CNRS-UVSQ, Institut Pierre Simon Laplace, Université Paris-Saclay, 91191 Gif-sur-Yvette, France*

[3] *Centre National de Recherches Météorologiques, Université de Toulouse, UMR 3589 CNRS/Météo-France, Toulouse, France.*

[4] *Sorbonne Université, CNRS, IRD, MNHN, Laboratoire d'Océanographie et du Climat (LOCEAN/IPSL), 4 place Jussieu, Paris F-75005, France.*

Contact: alina.gainusabogdan@gmail.com

Abstract

The mid-Holocene (6,000 years before present) was a warmer period than today in summer in most places of the Northern Hemisphere. In winter, over Europe, reconstructions of temperature based on pollen data show a dipole of temperature anomalies as compared to present-day, with warmer conditions in the north and colder in the south. It has been proposed that this pattern of temperature anomaly could be explained by a persisting positive phase of the North Atlantic

Oscillation during this period, which was, however, not reproduced in general by climate models. Indeed, PMIP3 models show a large spread in their response to the mid-Holocene insolation changes, the physical origins of which are not understood. To improve the understanding of the reconstructed temperature changes and of the PMIP3 model spread, we analyze the dynamical response of these model simulations in the North Atlantic for mid-Holocene conditions as compared to pre-industrial. We focus on the European pattern of temperature in winter, which allows comparing the simulations with a pollen-based reconstruction. We find that some of the model simulations yield a similar pattern to the reconstructed one, with lower amplitude, but which remains within the reconstruction uncertainty. We attribute the northern warm part of the latitudinal dipole of temperature anomaly in winter to a lower sea-ice cover in the Nordic Seas. The decrease of sea ice in winter indeed reduces the sea-ice insulation effect there, allowing the ocean heat released in winter to reach the continental northern Europe. This decrease in winter sea-ice cover is related to an increase in the Atlantic meridional overturning circulation (AMOC) and its associated ocean heat transport, as well as the effect of insolation changes on sea ice in summer, which persists until winter. Concerning the cooling of southern Europe, we only find a slight cooling signal mainly related to the insolation-induced cooling in winter over Africa. We show that the models that failed to reproduce any AMOC increase under mid-Holocene conditions are also the ones that do not reproduce the temperature pattern over Europe. The change in sea level pressure is not sufficient to explain the spread among the models. The ocean-sea ice mechanisms that we proposed constitute an alternative explanation to the pattern of changes in winter temperatures over Europe in the mid-Holocene, which is in better agreement with available model simulations of this period. Finally, we argue that this period can provide interesting emerging constraints on key changes in European climate, and indirectly of AMOC response to radiative changes.

Keywords: PMIP3, Mid-Holocene, NAO, AMOC, inter-model spread

Introduction

Projections of the climate of Europe show a large spread for the ongoing century (IPCC Working Group 1 et al. 2013). For a given emission scenario, uncertainties are related to the internal variability, that can be large at the regional scale (Deser et al. 2012), and to the model-dependent sensitivity of the climate system to external forcings (Hawkins and Sutton 2009). In particular, changes of the atmospheric or oceanic circulation tend to vary a lot between models. Future projections of the North Atlantic Oscillation (NAO), that plays a crucial role in the climate variability of Europe in winter (Hurrell 1995), do not even agree on its sign (Cattiaux and Cassou 2013). At multi-decadal timescales, the Atlantic Meridional Overturning Circulation (AMOC) also plays a key role for the climate of Europe through its massive northward transport of heat all along the Atlantic Ocean (Swingedouw et al. 2009, Haarsma et al. 2015, Jackson et al. 2015). Its long-term projections are, similarly, very uncertain (Weaver et al. 2012), even though all the models agree that it should decrease in the coming century, especially when the Greenland ice sheet melting is accounted for (Bakker et al. 2016; Swingedouw et al. 2015b). To improve our estimate of the response of the NAO or the AMOC to external forcing, paleoclimate data could provide key observational constraints (Schmidt et al. 2014; Harrison et al. 2015).

Paleoclimate reconstructions are based on proxy records that have been collected for decades around the world. The main issue with proxies is that they are indirect records of climate variables, so that they could be subject to large uncertainties and biases. Nevertheless, except for the short instrumental era, they are the only observational estimates of the climate response to different external forcings. Even though there is no exact analogue of the future in the past, information on the climate response to changes in external forcings has a high relevance to

74 better evaluate the sensitivity of climate models and possibly reduce the uncertainty concerning
75 the on-going climate change (Schmidt et al. 2014), especially at the regional scale.

76 The mid-Holocene (MH: 6000 years Before Present) is a recent period where the climate of the
77 northern high latitudes was considerably warmer than today in summer (Fischer et al. 2018),
78 due to a different insolation forcing (Figure 1). This is an interesting climate period, when the
79 Sahara is suspected to have been greener than today (Claussen and Gayler 1997). This is notably
80 why the Paleoclimate Model Intercomparison Project, phase 3 (PMIP3) initiative (Braconnot
81 et al. 2012) proposed this period as a key snapshot to be simulated by the same climate models
82 that produce climate projections (Schmidt et al. 2014; Harrison et al. 2015).

83

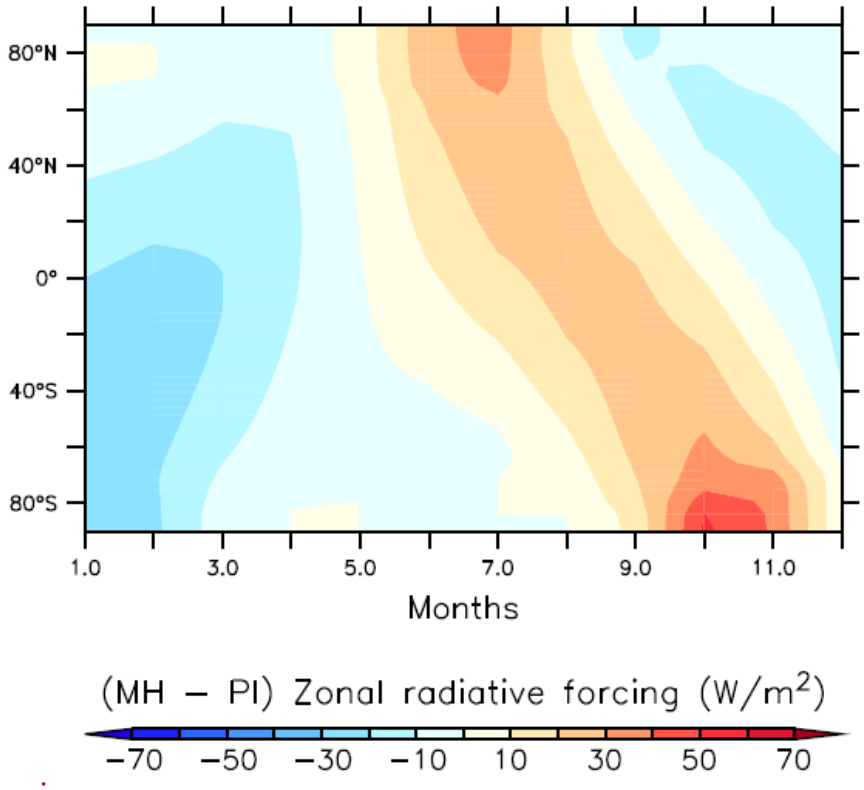

84

85 **Figure 1:** Zonally-averaged climatological monthly differences in the incoming shortwave radiation at the top of
86 the atmosphere between mid-Holocene and pre-industrial simulations.

87 A recent study proposed an improved reconstruction of climate over Europe for the MH based
88 on a broad compilation of pollen data (Mauri et al. 2014). The results showed a dipole of winter

near-surface temperature anomalies, with warm anomalies in the north of Europe and cold anomalies in the south. The authors suggested this pattern could be caused by an atmospheric circulation anomaly similar to a positive phase of the North Atlantic Oscillation (NAO^+). Other studies also proposed such a change for mid-Holocene European climate in winter (Guyard et al. 2013; Chabaud et al. 2014). This hypothesis therefore provides an interesting testbed for climate models. Mauri et al. (2014) argued that PMIP3 simulations in general did not reproduced very well the reconstructed dipole in temperature in winter because they not show any NAO^+-like changes in atmospheric circulation for the MH. This was also the case for the older PMIP2 dataset (Gladstone et al. 2005). Nevertheless, It have been proposed that PMIP2 dataset still showed some skill in capturing the pattern of climate change over Europe for the MH (Brewer et al. 2007). While the new generation of PMIP3 models show larger changes in sea ice for MH conditions than PMIP2 models over the Arctic (Berger et al. 2013), which may impact the response over Europe, a quantitative comparison of the PMIP3 models with winter reconstruction of temperature over Europe has not been made yet. Furthermore, a detailed analysis of the mechanism explaining the wintertime response in PMIP3 simulations for MH is also missing for the North Atlantic.

The large increase in summer insolation for MH conditions may have strongly affected the sea ice in polar regions, even in winter through inertia. This could then influence the continental climate, notably in winter where the heat flux release by the ocean is largest, as well as the insulation effect of sea ice (Goosse et al. 2002). Such an impact was illustrated by Fischer and Jungclaus (2011) in a transient simulation over part of the Holocene using the MPI climate model. Otto et al. (2009), using different simulations for the MH including a coupling to the ocean and vegetation or not, also showed that the ocean plays a key role for the amplitude of the temperature response of the northern high latitudes to the radiative forcing. The insolation during the MH was indeed very different from the pre-industrial period. The latitudinal gradient

was strongly reduced during the summer season, which could have impacted the oceanic and atmospheric meridional heat transport (Davis and Brewer 2009).

In the present study, we propose to analyze the response of climate models participating to PMIP3 under MH wintertime conditions, with a specific focus on the North Atlantic region. We will assess the potential causes for the model spread in temperature response over Europe in winter and analyze the role played by changes in atmospheric circulation, oceanic circulation and radiative changes amplified by sea ice response. We will also compare these simulations, using classical skill scores, with the reconstruction of Mauri et al. (2014). This will allow us to determine the models that best reproduce the temperature dipole pattern over Europe. Our main result is that atmospheric circulation changes are not the main driver of the simulated patterns of temperature anomalies. These are instead linked to sea-ice anomalies, forced either by AMOC slowdown or summer sea-ice melt.

Experimental design

We analyze pairs of mid-Holocene and pre-industrial (PI) simulations performed with PMIP3 climate models. Only 12 models (Table 1) are retained, as we require at least 100 years of both PI and MH simulations to perform robust statistical analyses. When more than 200 model years are available, we use the last 200 years of the simulation. Throughout the analyses, we use data on the native grid for each model, except when multi-model statistics are calculated, in which case the model data is first interpolated on a regular 1°x1° grid for the temperature to be compared with Mauri et al. (2014) and a regular 2.5°x2.5° grid for the other variables.

Index	Model	Modeling Center	Reference
A	bcc-csm1-1	Beijing Climate Center (BCC)	Xin et al. (2013)
B	CNRM-CM5	Centre National de Recherches Météorologiques/ Centre Européen de Recherche et Formation Avancées en Calcul Scientifique (CNRM/CERFACS)	Voldoire et al. (2013)
C	CSIRO-Mk3-6-0	Commonwealth Scientific and Industrial Research Organization/ Queensland Climate Change Centre of Excellence (CSIRO-QCCCE)	Rotstayn et al. (2012)
D	IPSL-CM5A-LR	Institut Pierre-Simon Laplace (IPSL)	Dufresne et al. (Dufresne et al. 2013)
E	FGOALS-g2	State Key Laboratory of Numerical Modeling for Atmospheric Sciences and Geophysical Fluid Dynamics/Institute of Atmospheric Physics (LASG/IAP)	Li et al. (2013)
F	FGOALS-s2	LASG/IAP	Bao et al. (2013)
G	MIROC-ESM	Atmosphere and Ocean Research Institute (The University of Tokyo), National Institute for Environmental Studies, and Japan Agency for Marine-Earth Science and Technology	Watanabe et al. (2011)
H	HadGEM2-ES	Met Office Hadley Center (MOHC)	Collins et al. (2011)
I	MPI-ESM	Max Planck Institute for Meteorology (MPI-M)	Jungclaus et al. (2013)
J	MRI-CGCM3	Meteorological Research Institute (MRI)	Yukimoto et al. (2012)
K	GISS-E2-R	NASA Goddard Institute for Space Studies	Schmidt et al. (2006)
L	CCSM4	National Center for Atmospheric Research (NCAR)	Gent et al. (2011)

Table 1: List of PMIP3 models included in this study.

We focus our analysis on Mid-Holocene climatological anomalies with respect to the pre-industrial period for wintertime (December-February averages – DJF), summertime (June-August averages – JJA) or annual means (ANM). Wherever suitable, we use a two-sided

independent sample t-test to determine if and to what level these anomalies are statistically significant, considering the interannual variability in the PI and MH simulations, at each grid point. Where this is done, we shade in color the regions where the anomalies are significant at the 90% confidence level. For a more stringent test, we add contours corresponding to significant anomalies at the 99% confidence interval.

Temperature and circulation response

MH winter temperature response in PMIP3 models

While the external forcing (insolation changes) is the same in the different models, their responses to MH climatic condition in winter over Europe are very different, as shown in Figure 2. This figure shows the significant winter surface atmospheric temperature (SAT) anomalies over Europe simulated with the 12 different climate models, the multi-model ensemble mean anomaly and the reconstruction by Mauri et al. (2014). The uncertainties in the pollen-based reconstruction can be quite large, therefore Figure 2n only shows those $\Delta SAT_{DJF,EU}$ values that are larger in absolute value than the respective estimated uncertainties. We find a wide range of simulated SAT anomaly patterns between the 12 models, and some important differences from the mean reconstructed pattern. We quantify these model-reconstruction differences in Figure 3, showing the pattern correlation, pattern root-mean-square difference (RMSE; pattern RMSE obtained by removing the respective spatial average from each field before the RMSE calculation) and full-field RMSE for each model compared to the Mauri et al. (2014) reconstruction, as well as for the multi-model ensemble mean.

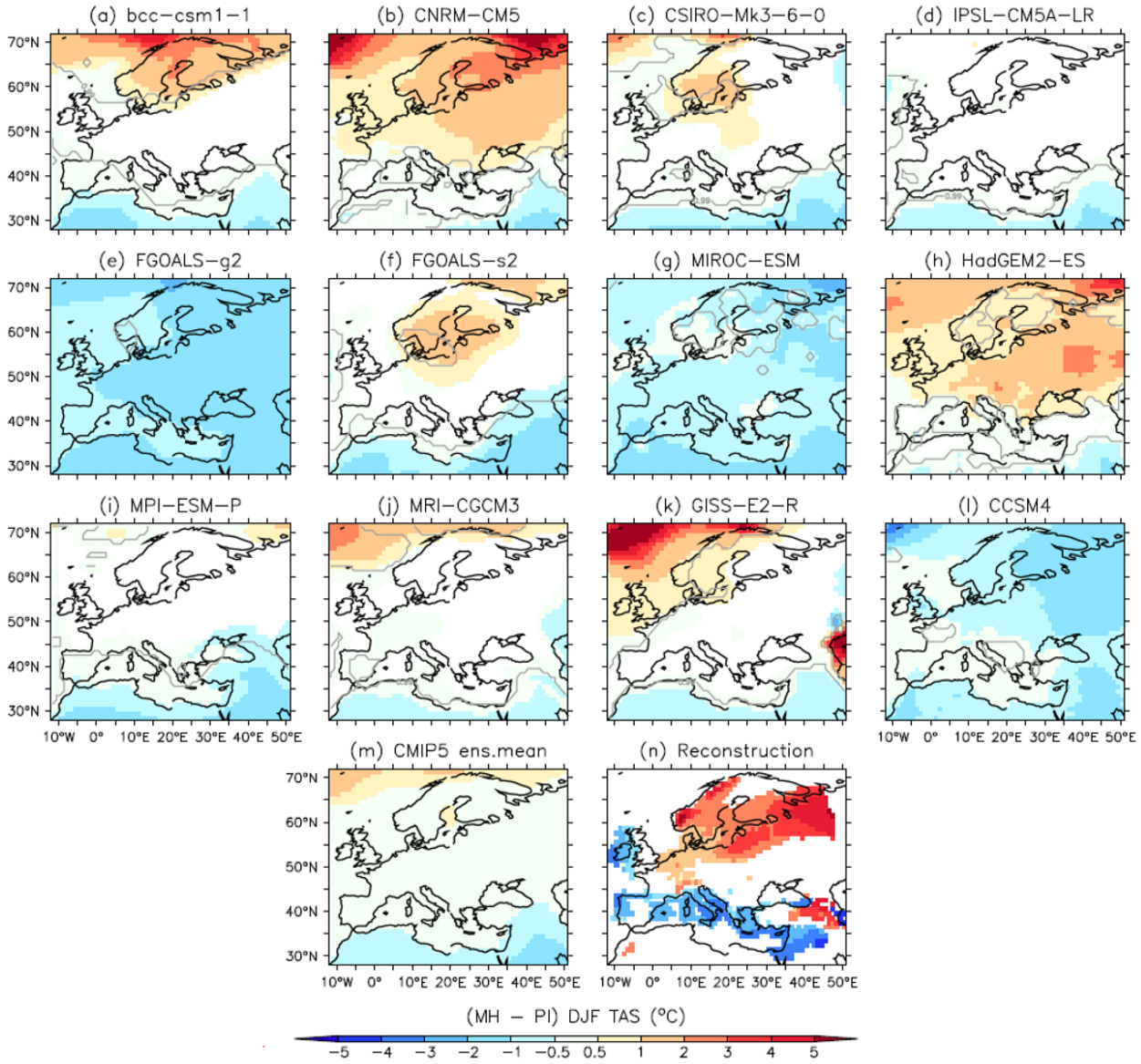

Figure 2: (a)-(l) Significant differences (color: at 90% confidence level; inside contours: at 99% confidence level) between mean wintertime near-surface air temperature (SAT) in mid-Holocene and pre-industrial simulations run with 12 different climate models; (m) Multi-model ensemble mean difference between MH and PI climatological wintertime SAT; (n) Mauri et al. (2014) reconstruction of the MH climatological wintertime SAT anomaly – only data where the signal is larger than the estimated uncertainty is considered.

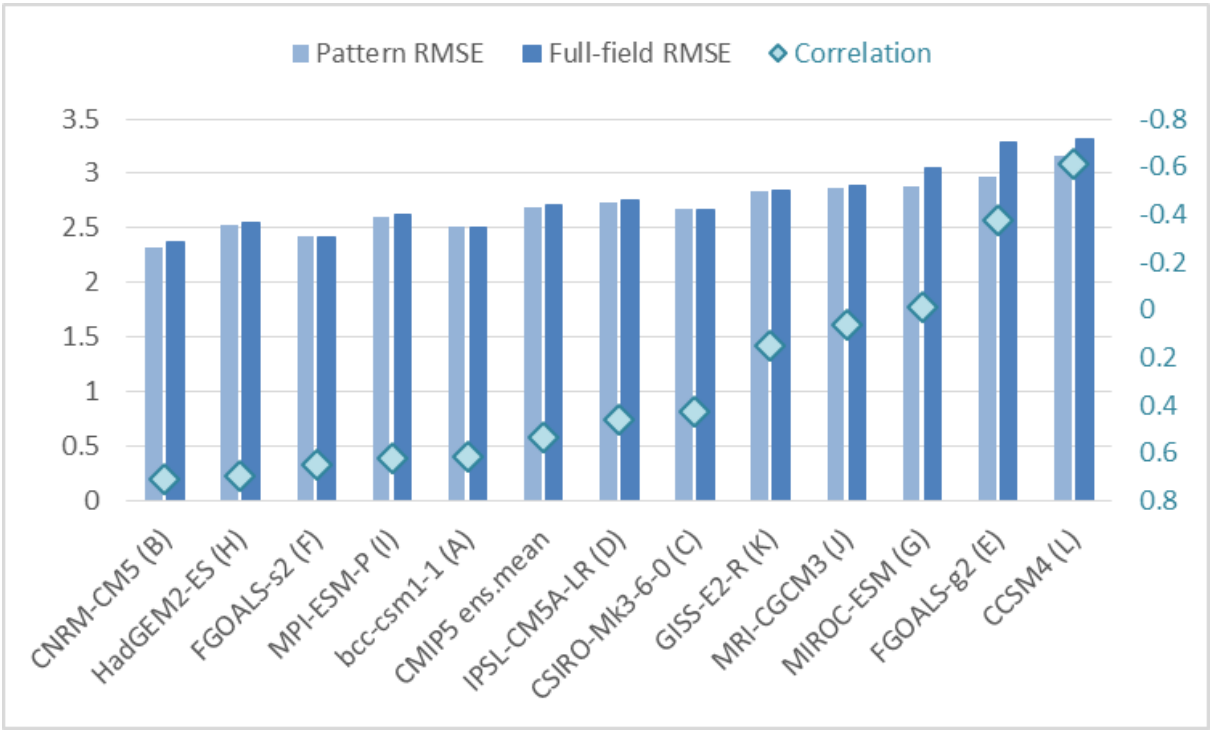

Figure 3: Statistics comparing the simulated and reconstructed (Mauri et al. 2014) mid-Holocene wintertime SAT anomalies over Europe. Correlation (values shown on the right-side vertical axis): spatial correlation coefficient between the two fields compared; Pattern RMSE: root-mean-square error when the respective spatial average has been removed from each of the two fields compared; Full-field RMSE: total root-mean-square-difference between the two fields. The model data, including the multi-model ensemble mean, are sorted from the highest to the lowest spatial correlation with the reconstructed data. The statistics are only calculated using those grid points where the reconstructed signal is stronger than the estimated uncertainty (see Figure 4n).

Some models fail to represent the reconstructed $\Delta SAT_{DJF,\,EU}$ pattern, like CCSM4, FGOALS-g2 and MIROC-ESM, which show near-zero or negative spatial correlation coefficients with the reconstructed field and RMSEs larger than 3°C. Other models like CNRM-CM5 and HadGEM2-ES have some success in simulating a similar pattern, *i.e.*, a positive north-south temperature anomaly gradient (spatial correlation coefficient ~0.7) but still fail at simulating the reconstructed amplitude (pattern RMSE $\geq$ 2.3°C), and the temperature anomalies themselves (full-field RMSE $\geq$ 2.4°C).

MH winter atmospheric circulation anomalies in the PMIP3 models

Mauri et al. (2014) proposed that the MH temperature anomaly pattern over Europe could be caused by a NAO-like atmospheric circulation anomaly. To explore this possibility in the PMIP3 database, Figure 4 shows the statistically significant sea-level pressure differences (ΔSLP) between the climatological wintertime (DJF) MH and PI simulations over the North Atlantic (NA) sector for the 12 analyzed models. All models show significant MH winter SLP anomalies, of the order of 0.5-1.5 hPa, with corresponding 1000-hPa wind speed anomalies ($\Delta U_{horiz,DJF,1000}$, not shown) of the order of 0.2-0.7 m/s.

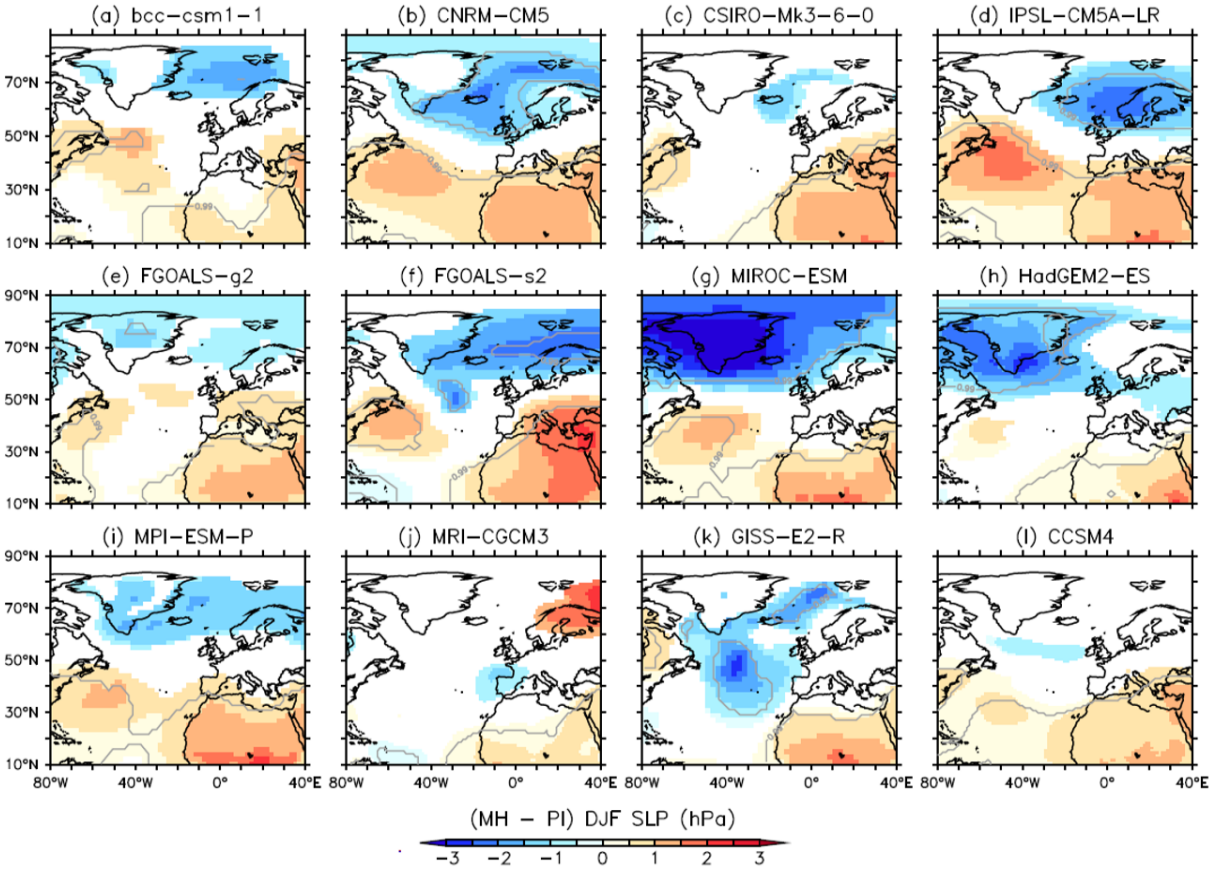

Figure 4: Significant differences (color: at 90% confidence level; inside contours: at 99% confidence level) between mean wintertime sea-level pressure in mid-Holocene and pre-industrial simulations run with 12 different climate models.

Figure 5 shows the multi-model mean circulation anomalies at different levels in the troposphere. Significant anomalies are found at all atmospheric levels. The most notable feature is a negative zonal wind speed anomaly in the subtropics (around 30^{o}N), maximum at upper levels (Δu_{200}) and over the western half of the North Atlantic. This feature is present in all models, but with structures varying in strength, extent and zonal orientation. We can trace it to a local weakening of the jet streams (in some models, accompanied by a slight northward shift of the eddy-driven jet) and, for most models, a more marked separation between the eddy-driven and subtropical jet streams over the North Atlantic (illustrated in Figure 5a for the multi-model ensemble mean). This results in an anticyclonic horizontal wind speed anomaly and local high pressure in the West Atlantic northward of the negative Δu_{200} region. For most models, this anticyclonic anomaly dominates the pattern of mean atmospheric circulation change over the North Atlantic. In those cases, this anomaly structure is found throughout the atmospheric column (as illustrated in Figure 5c for the 500 hPa level), down to the surface (Figure 5e), explaining the positive SLP anomalies found in most models over the southwestern North Atlantic (Figure 4, Figure 5d). Even the MRI model, which has no significant anomalies in the lower atmosphere, shows a similar significant anomaly in the jet stream.

While this positive pressure anomaly in the Western Atlantic has an equivalent barotropic structure that extends throughout the troposphere, the positive SLP anomaly seen over North Africa in the multi-model mean (Figure 5d) is on the contrary very shallow, disappearing or even changing sign at 500 hPa. This baroclinic structure is linked to a cold temperature anomaly in the atmospheric column, which can be explained by the negative DJF radiative forcing. The reduction of the radiative forcing is strongest at low latitudes (Figure 1), and has a larger impact over continental regions like North Africa.

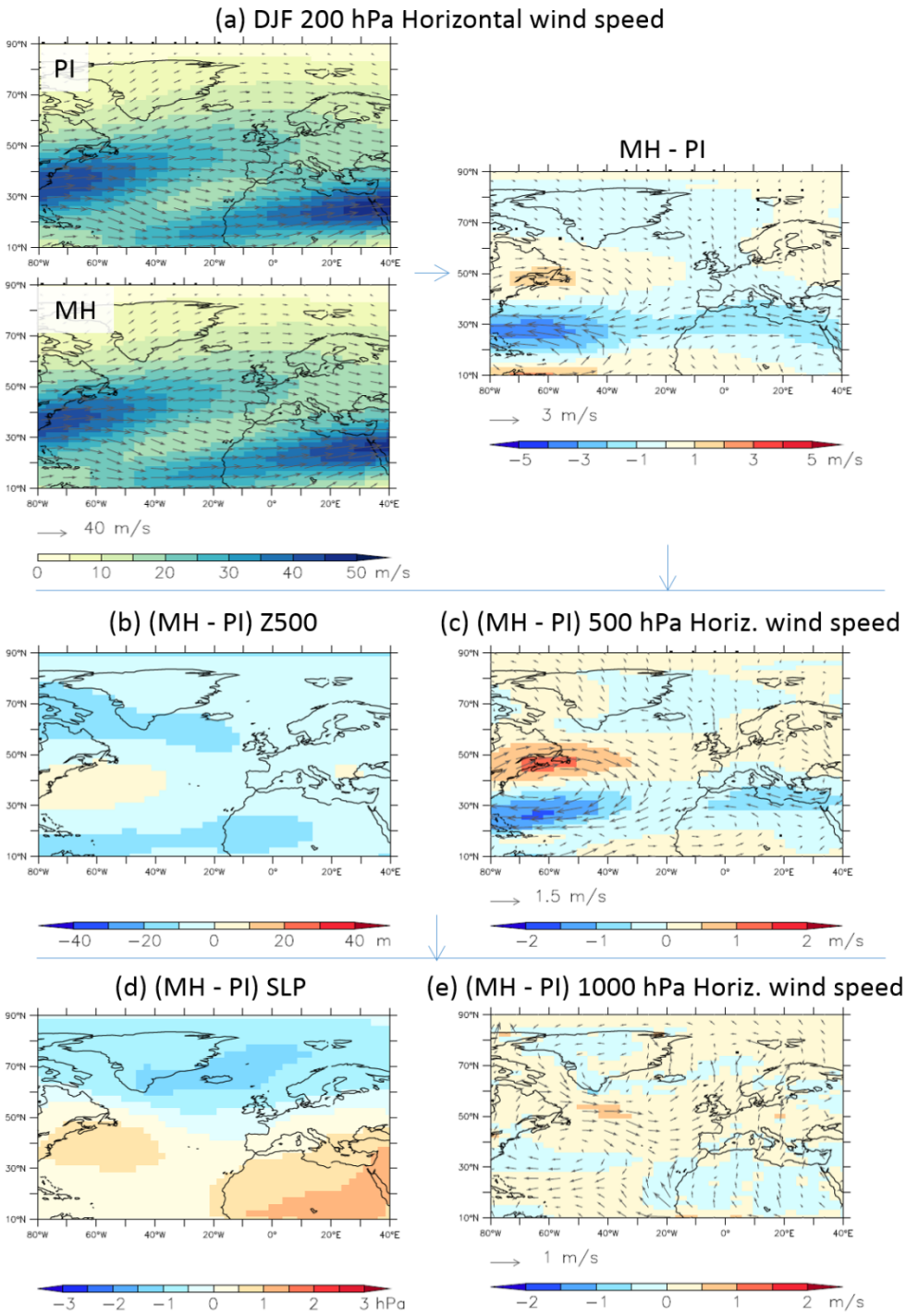

219

220 Figure 5: Multi-model ensemble mean wintertime: (a) 200 hPa horizontal wind speed in pre-
221 industrial (PI), mid-Holocene (MH) simulations and the corresponding MH-PI difference; (b)
222 500 hPa geopotential height MH anomaly; (c) 500 hPa horizontal wind speed anomaly; (d)
223 sea-level pressure anomaly; (e) 1000 hPa horizontal wind speed anomaly.

Atmospheric circulation vs. European temperature anomaly patterns

Figure 4 shows that several PMIP3 models simulate a positive SLP anomaly over the southern part of the North Atlantic and a negative SLP anomaly over the northern part of the basin during MH winters. This pattern could be roughly construed to be NAO^+-like, as Mauri et al. (2014) argued could cause their reconstructed DJF ΔSAT_{EU} pattern. This section examines whether such a relationship between a NAO^+-like circulation anomaly and a ΔSAT_{EU} pattern can be found within our multi-model ensemble.

A key question is whether the differences between the simulated temperature anomaly patterns between models can be attributed to the differences in their simulated atmospheric circulation anomalies over the North Atlantic. More specifically, we want to assess whether the models that simulate a positive north-south temperature gradient over Europe are only the models that also simulate a NAO^+-like circulation anomaly over the North Atlantic.

A qualitative comparison of Figure 2 and Figure 4 indicates that this is not the case. While the hypothesis of a NAO^+-like cause of marked north-south gradients in $\Delta SAT_{DJF,\ EU}$ could hold for a few models (*e.g.*, CNRM-CM5), the ensemble of models does not support it. Some models exhibit a NAO^+-like circulation without a strong north-south $\Delta SAT_{DJF,\ EU}$ gradient (*e.g.*, IPSL-CM5A-LR, MIROC-ESM), while other models show a marked $\Delta SAT_{DJF,\ EU}$ gradient without simulating a NAO^+-like circulation anomaly (*e.g.*, GISS-E2-R). For some model simulations showing a negative SLP anomaly around Iceland, which can look like part of a NAO^+ pattern, just like over Africa the pressure anomaly disappears with height (not shown), and is most likely a thermal structure caused by the local warming at the surface.

For a quantitative assessment, Figure 6 evaluates the relationship between first-order indices of the large-scale temperature and circulation changes, namely the north-south $\Delta SAT_{DJF,\ EU}$ gradient and the NAO^+-like ΔSLP_{NA}. The north-south $\Delta SAT_{DJF,\ EU}$ gradient is defined as the

mean temperature difference between a northern and a southern region over Europe chosen to approximately reflect the Arctic Oscillation signature on SAT_{EU}, as shown in Mauri et al. (2014 - top left panel in Figure 6). The NAO^+-like ΔSLP_{NA} is defined as the mean sea-level pressure difference between regions chosen to approximately reflect the centers of action of the North Atlantic Oscillation index (*cf.* Hurrell & Deser 2010 – bottom right panel in Figure 6). The scatterplot between the two indices in the top right panel of Figure 6 shows a lack of significant correlation that confirms that the PMIP3 models do not support a straightforward link between MH temperature anomaly patterns over Europe and a NAO^+-like circulation anomaly over the North Atlantic.

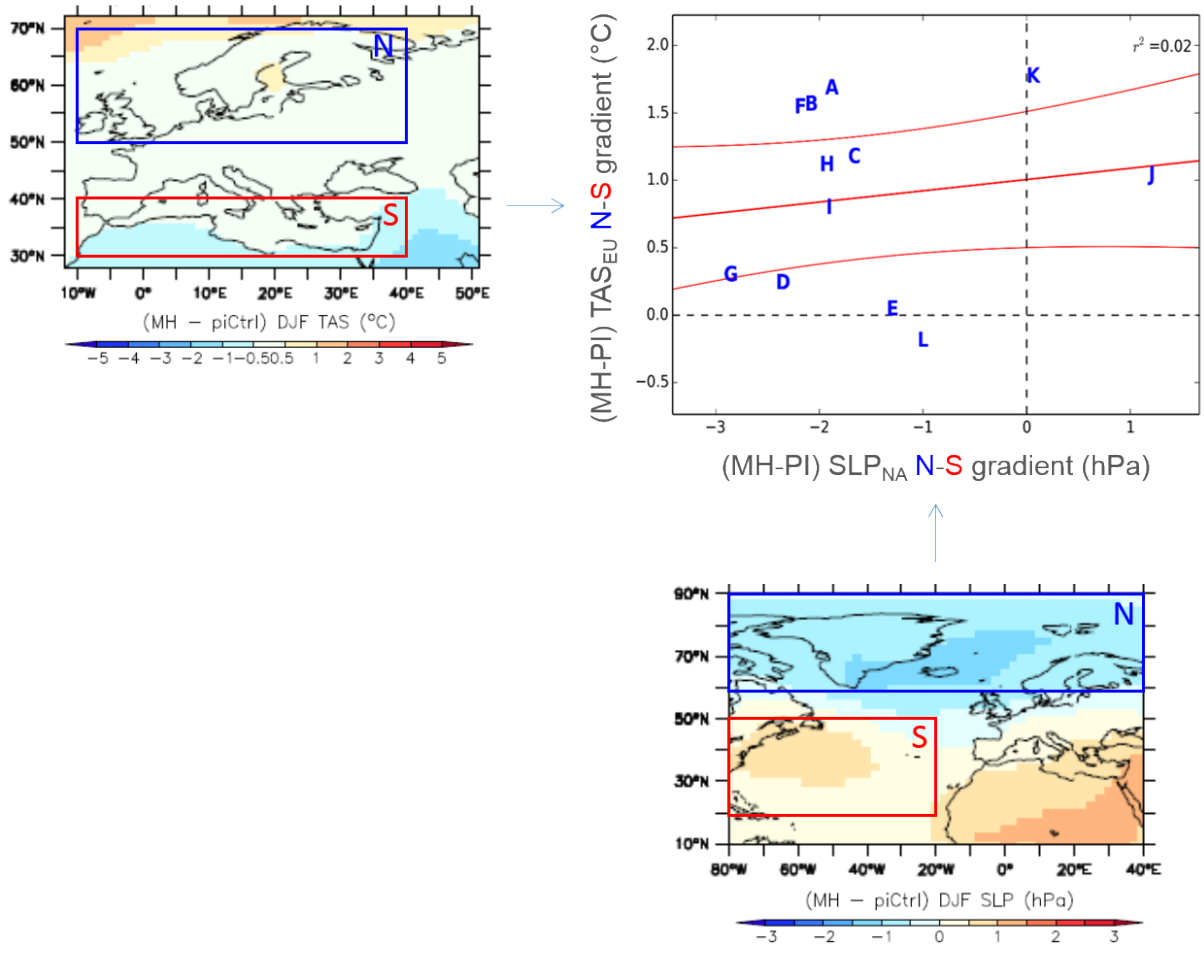

Figure 6: Top left: PMIP3 ensemble mean anomalies of SAT (in °C) in DJF for MH minus PI. The blue box defines the northern region and the red box, the southern region used for calculating the north-shout SAT gradient. Bottom right: PMIP3 ensemble mean anomalies of SLP (in hPa) in DJF for MH minus PI. The blue box defines

the northern region and the red box, the southern region used to define the SLP north-south gradient. Top right: Multi-model relationship of the land temperature anomaly gradient (defined in top left panel) - on the y-axis - and the SLP anomaly gradient (defined in bottom right panel) - on the x-axis. The squared correlation coefficient is shown in the top-left corner of the figure. The red lines indicate the linear regression and the 95% confidence interval for this regression.

Factors determining the simulated $\Delta SAT_{DJF,EU}$ meridional gradients

Figure 2 shows that the strongest $\Delta SAT_{DJF,\ EU}$ signals are found, for most models, close to the latitude boundaries of the region considered. Enlarging the domain of our analysis places the European temperature anomalies patterns in the larger-scale context (Figure 7a). We find that the modeled north-south $\Delta SAT_{DJF,\ EU}$ contrasts are dominated, to the north, by warm temperature anomalies over the Nordic Seas and, to the south, by cold temperature anomalies over northern Africa.

To a large extent, the negative SAT anomalies over northern Africa (and the positive SLP anomalies) are related to the negative radiative forcing in winter at these latitudes (Figure 1). This anomaly is strongest at low latitudes and has an amplified effect on SAT over continents vs. oceanic regions, possibly due to the lower heat capacity of land than water.

Inter-model differences of ΔSAT over the southern region in Figure 5 are indeed small (0.3^{o}C inter-model standard deviation) relative to the ones over the northern region (0.8^{o}C), consistent with a lower ΔSAT inter-model standard deviations over northern Africa than over the Nordic Seas (Figure 7b). Thus, for the rest of the paper we will focus mainly on what determines the inter-model spread in ΔSAT_{DJF} over the Nordic Seas, that dominates the north-south contrast.

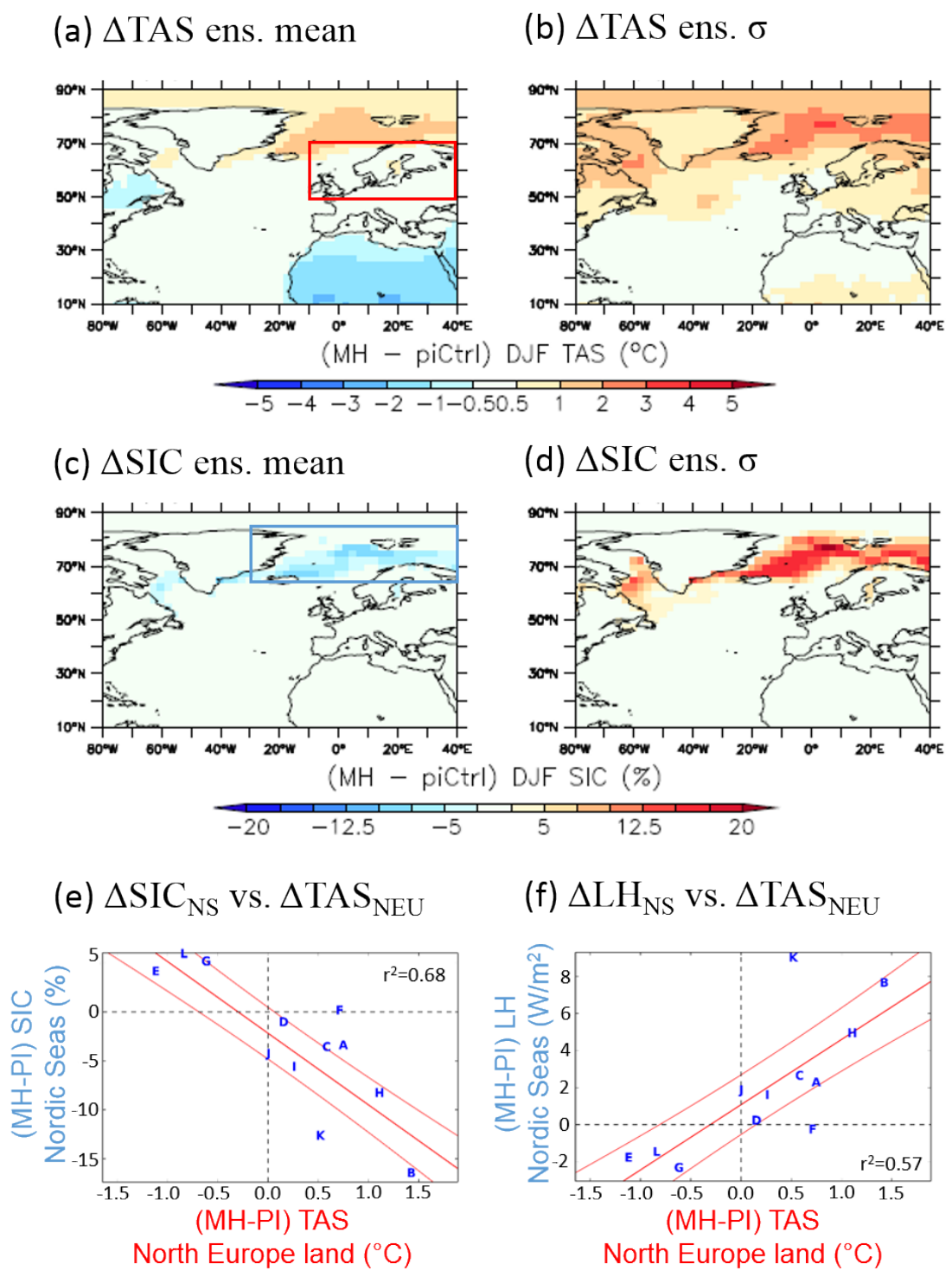

Figure 7: MH winter anomalies of (a, b) near-surface air temperature and (c- d) sea ice cover over the North Atlantic sector. (a) and (c) show the multi-model ensemble mean anomalies and (b) and (d) show the ensemble standard deviation. (e) Relationship between simulated near-surface air temperature over land in northern Europe and sea ice cover anomalies averaged over the region highlighted in (a) and (c) for the 12 models analyzed. (f) Same as (e) but with sea ice cover anomalies replaced by latent heat flux anomalies from the ocean to the

atmosphere. The squared correlation coefficient is show in the top- and, respectively, bottom-left corner of the plots. In both plots, the red lines indicate the linear regression and the 95% confidence interval for the regression.

The spatial patterns of both the ΔSAT_{DJF} signal in the Nordic Seas and its inter-model spread (Figure 7a, b) are strongly reminiscent of those of the DJF sea-ice cover anomalies (Figure 7c, d). Sea-ice cover changes have a strong impact on near-surface temperatures *via* air-sea fluxes and albedo feedbacks (Swingedouw et al. 2006, Årthun et al. 2017). This influence extends to neighbouring land regions: the inter-model differences in ΔSAT_{DJF} in land areas of northern Europe (Figure 7e) are well correlated (r^2=0.68, $p<0.01$) with the differences in ΔSIC_{DJF} over the Nordic Seas. Furthermore, these differences in ΔSAT_{DJF} are also well correlated with the changes in latent heat flux from the ocean to the atmosphere over the Nordic Seas. Thus, we argue that it is the difference in latent heat flux released in winter by the ocean to the atmosphere and associated with the insulation effect of the presence (or not) of sea ice that explains the response of ΔSAT_{DJF} over northern Europe land. A similar mechanism was indeed highlighted by Årthun et al. (2017) to explain the impact of Nordic Seas SST variability on the temperature of Scandinavia.

Thus, to understand the differences between the wintertime MH European temperature anomalies between the models, we mainly need to understand the origins of the differences between the simulated sea ice cover anomalies in the Nordic Seas region.

Origins of winter sea-ice decline

Atmospheric circulation anomalies

While NAO-like anomalies do not directly determine the inter-model differences in winter temperature anomalies over Europe in PMIP3 ensemble, atmospheric circulation changes between MH and PI winters could potentially control the sea ice anomalies in the Nordic Seas, through anomalous atmospheric heat transport.

To test this hypothesis, we tried to calculate the total atmospheric heat transport into the Nordic Seas region. This computation should be based on changes of both the mean and transient circulation. Unfortunately, the PMIP3 database does not routinely include data at sufficiently high frequencies to allow for the calculation of the latter term, nor does it provide estimates of atmospheric heat transport computed at the model time step. We can thus only offer a partial answer, related to the mean wind anomalies only.

Whether we consider the near-surface horizontal temperature advection due solely to the change in the mean winter near-surface horizontal wind velocities between PI and MH (estimated as $-\Delta\vec{U}\cdot\nabla T_{PI}$, where Δ stands for MH-PI differences, $\vec{U}$ for the horizontal wind velocity and T_{PI} for the temperature for pre-industrial simulation; Figure 8) or the change between the mean circulation-induced horizontal temperature advection in PI vs. MH winters (estimated as $-\Delta(\vec{U}\cdot\nabla T)$; not shown), we find no correlation of these respective anomalies with the winter sea ice cover anomaly over the Nordic Seas region (Figure 8). More generally, two other elements of the energy budget argue against an increased poleward atmospheric transport in MH winter: at the top of the atmosphere, the latitudinal gradient of insolation decreases (with more cooling at lower latitudes), and the ocean heat transport tends to increase (due to AMOC strengthening as shown below). Both would typically lead to a compensating equatorward energy transport by the atmosphere, away from the sea ice region. Such a response has actually been demonstrated in MH simulations run with the IPSL-CM5A-LR model (Saint-Lu et al. 2016). We thus find no evidence that the changes in the atmospheric heat transport may be responsible for ΔSIC_{DJF} in the models.

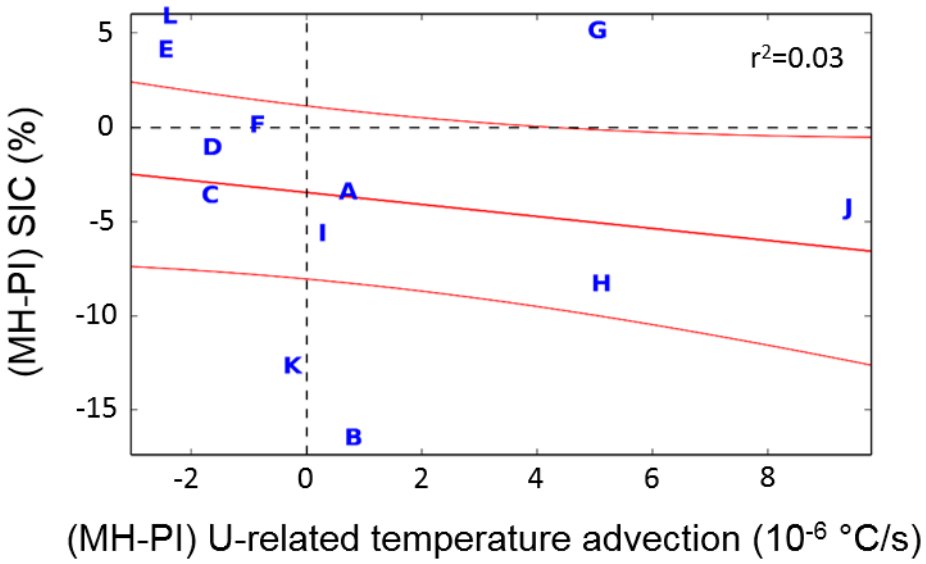

333

334 **Figure 8:** Multi-model relationship between wintertime sea ice cover anomalies and mean 1000hPa horizontal
335 circulation anomaly-related temperature advection in the NS region. The red lines indicate the linear regression
336 and the 95% confidence interval for this regression.

337 ## Summer sea ice anomalies

338 Another potential source of the inter-model differences in winter sea ice anomalies is the
339 summer (JJA) sea ice response, with a memory effect between the two seasons. Indeed, the
340 insolation is far larger in the Mid-Holocene compared to the pre-industrial period during
341 summer (Figure 1), potentially leading to large melting of sea ice and heat storage in the ocean
342 in summer, which may then persist into winter due to the large inertia of the ocean. There is a
343 fine interplay between winter and summer sea ice: winter sea ice thickness heavily influences
344 the ice pack vulnerability to summer melt, and thus has an important effect on summer sea ice
345 cover (Berger et al. 2013). Conversely, summer melt allows for ocean surface heat uptake and
346 renders new sea ice formation more difficult during autumn and winter. Thus, we can also
347 expect a ΔSIC_{JJA} effect on ΔSIC_{DJF} (Berger et al. 2013). This latter effect may play an important
348 role in determining the inter-model ΔSIC_{DJF} differences. Indeed, the different models may
349 exhibit different sea ice responses to the summer radiative forcing (Figure 1) for example

through different strength of feedbacks, like the local cloud response (*cf.* Knudsen et al. 2015; Abe et al. 2015). These differences in summer may then project on the winter responses.

We thus check if the relationship between ΔSIC_{JJA} and ΔSIC_{DJF} is consistent between the models. Figure 9 indeed shows a strong multi-model relationship between ΔSIC_{JJA} and ΔSIC_{DJF}, both globally over the Northern Hemisphere high latitudes (r^2=0.74, p<0.01), and regionally over the Nordic Seas (r^2=0.73, p<0.01).

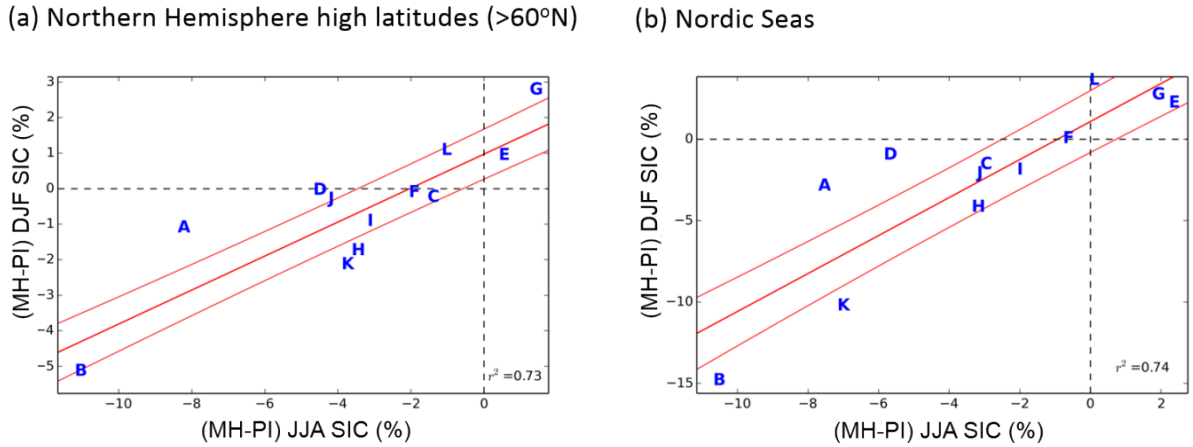

Figure 9: Relationship between MH winter and summer sea ice cover anomalies (a) averaged over the Northern Hemisphere high latitudes (above 60°N); (b) averaged over the Nordic Seas (rectangular region contoured in Figure 7a, c). The text boxes in the bottom-left corner of the figures show the associated squared correlation coefficients. The red lines indicate the linear regressions and the 95% confidence interval for the regressions.

While it is likely that a memory of the seasonally forced ΔSIC_{JJA} can influence ΔSIC_{DJF}, it is also possible that both summer and winter sea ice anomalies are influenced by a large-scale, common factor such as a change in the Atlantic meridional overturning circulation (AMOC), which we investigate in the following section.

Change in AMOC

Figure 10 shows the changes in the AMOC between the simulated MH and PI climates. All 12 models analyzed show significant anomalies in the mean AMOC, with considerable inter-

model variability in terms of both anomalies (Figure 10, colors) and background state (PI AMOC – Figure 10, contours). In general, the AMOC is strengthened in MH compared to PI. This is consistent with Born et al. (2010), who proposed that for a climate with warmer summer (the Eemian in their case), the decrease in sea ice transport through Fram Strait may change the salinity in the Labrador Sea and enhance local convective activity, feeding a stronger AMOC.

AMOC MH anomalies vary between models not just in terms of intensity, but also in terms of structure, complicating their quantitative comparison. Nevertheless, maxima of the meridional stream function have been shown to be strongly related to the meridional ocean heat transport (*e.g.* Boning et al. 1995). Thus, they represent a reasonable parameter to consider in the investigation of sea ice changes.

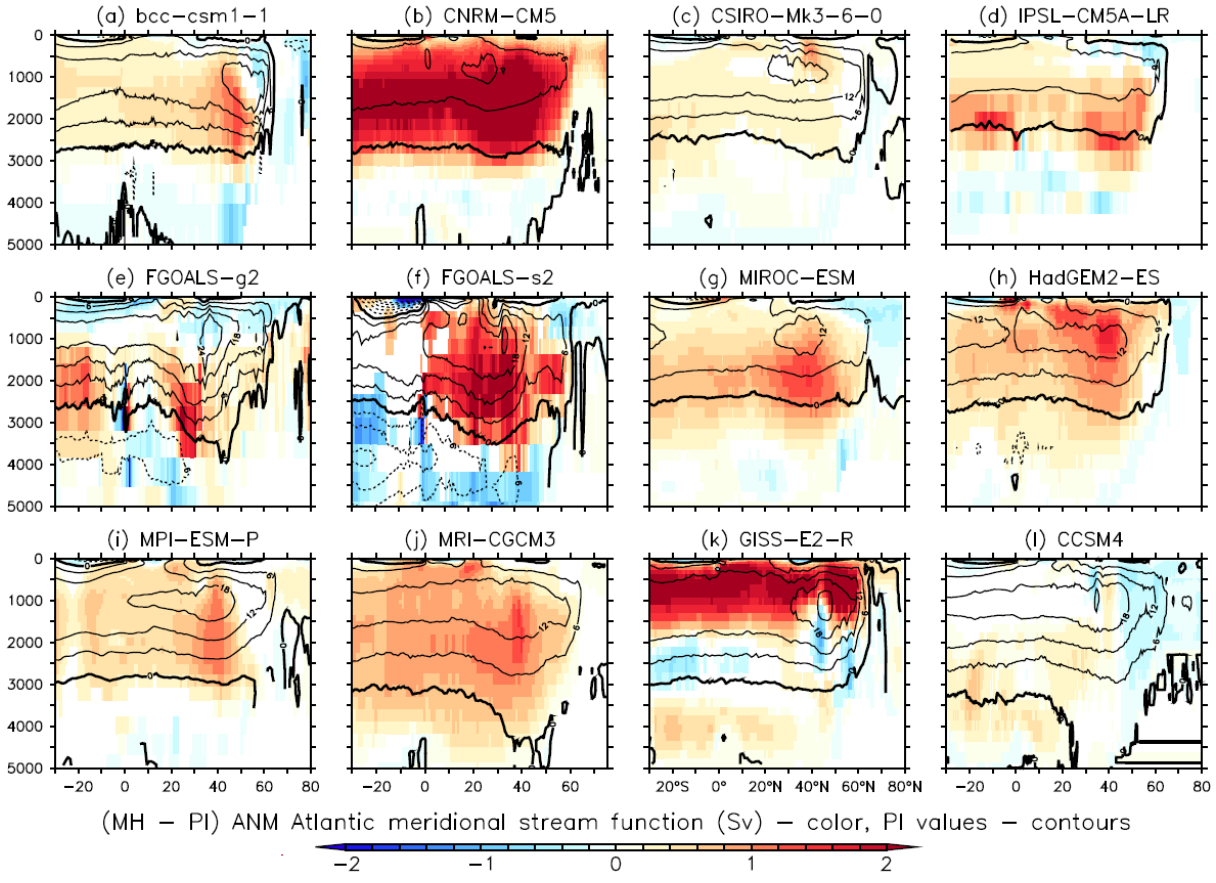

Figure 10: Color: significant (at 90% level) MH anomalies of the climatological annual mean (ANM) Atlantic meridional stream function; contours: PI climatologies (contour spacing: 6 Sv; solid/dashed contours represent positive/negative values) for the 12 models analyzed.

Figure 11 shows the relationship between winter sea-ice cover anomalies and anomalies in the maximum of the climatological Atlantic meridional stream function at three different latitudes: 26^{o}N and 45^{o}N, typically used when describing the AMOC strength (*e.g.*, Huck et al. 2008, McCarthy et al. 2015), and 60^{o}N, closer to the Nordic Seas region. The DJF SIC anomalies are in all cases negatively correlated with the AMOC strength anomalies. The correlation coefficient and the slope of the corresponding linear regressions increase with latitude, so that the strongest link of $\Delta SIC_{DJF,NS}$ with the meridional ocean circulation is found for ΔAMOC at 60^{o}N. The correlation coefficient is 0.89 (p-value < 0.01) and the linear regression line has a near-zero intercept, indicating that, as would be expected, an intensification of the AMOC at high latitudes is linearly associated to negative SIC anomalies in the Nordic Seas and *vice-versa*. The correlation remains high even at 26°N ($r=0.75$, $p<0.01$), indicating that this relationship is not a purely local effect.

Changes in the subpolar gyre may also strongly affect the heat transport to the high latitudes (Born et al. 2015). However, the barotropic stream function was not available for all the models, limiting the analysis of this effect. Since the strength of the subpolar gyre is closely related to the strength of the convection in the subpolar gyre (Born et al. 2015), we suggest that the changes in AMOC would also be reflected in subpolar gyre strength, both leading to an increase of meridional heat transport.

The changes in oceanic heat transport act on longer than seasonal time scales and may thus affect sea-ice cover in both winter and summer, likely contributing to the correlation between winter and summer anomalies highlighted in Section 6.2. Nevertheless, direct changes in summer sea ice in response to changes in insolation are also due to regional sensitivity and feedbacks that may differ among the models (*e.g.*, Massonnet et al. 2012), and so could remain a relatively independent factor from AMOC strengthening to explain the inter-model spread.

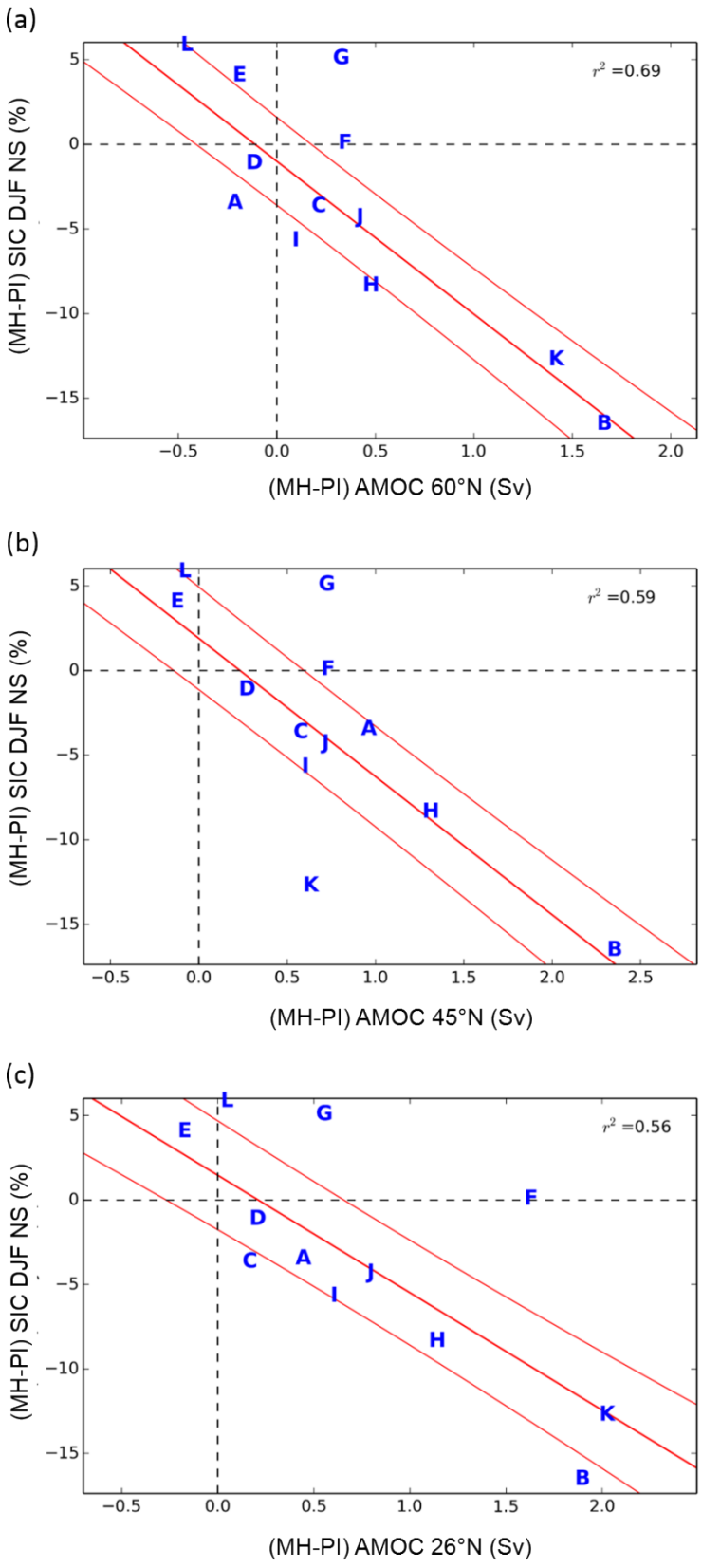

407

408 **Figure 11:** Relationship between mean winter MH sea ice cover anomalies over the Nordic Seas region and the
409 MH anomaly in the maximum climatological Atlantic meridional stream function at (a) 60°N, (b) 45°N and (c)
410 26°N. The squared correlation coefficients of the associated linear regressions are shown in the respective panels.

411 The correlations are significant above the 99% level. The red lines indicate the linear regression and the 95%
412 confidence interval for this regression.

413 Combination of multiple factors

414 In the previous subsections we have analyzed one-to-one relationships between $\Delta SIC_{DJF,NS}$ and
415 a suite of atmospheric and oceanic variables. However, the inter-model differences in the winter
416 sea ice anomalies are most likely explained by a combination of different factors which affect
417 the sea ice cover in different measures depending on the model.

418 We have investigated a wide array of variable combinations to best explain the inter-model
419 variations in $\Delta SIC_{DJF,NS}$ through multiple linear regressions. We have considered parameters
420 physically linked with the winter sea ice anomalies, like the temperature advection due to the
421 mean circulation change in the Nordic Seas region, the surface downward radiative flux
422 anomalies, the background state (PI) sea ice cover, the summer sea ice cover anomalies and the
423 change in the AMOC strength.

424 The low number of climate simulations (12), the reductive framework (lack of sensitivity
425 experiments) and the intrinsic high level of connectivity between climate variables through non-
426 linear relationships (i.e., variables not independent) limit the potential of such a multivariate
427 analysis. Nevertheless, some information can be distilled on the basis of this exercise.

428 While in most combinations and for most predictor variables, the high p values associated to
429 their respective coefficients did not allow for meaningful regressions, the p values associated
430 to the coefficient for the AMOC strength anomaly at 60^{o}N were always very small (on the order
431 of 10^{-4}-10^{-5}) and the coefficients themselves were always found to be negative, indicating a
432 robust effect of ΔAMOC on $\Delta SIC_{DJF,NS}$ in the direction already described in Section 6.4.

433 One multiple linear regression did yield significant results:

434

$$\Delta SIC_{DJF,NS} = \alpha_0 + \alpha_1 \Delta AMOC_{max.60^oN} + \alpha_2 \Delta SIC_{JJA,NS} \quad (1)$$

with $p_{\alpha_0} = 0.04$, $p_{\alpha_1} = 10^{-4}$, $p_{\alpha_2} = 4 \cdot 10^{-5}$ and an adjusted r^2 of 0.96.

Figure 12 shows the results of the multiple linear regression model in Eq. 1. Figure 12a shows the good correspondence between the reconstructed and original $\Delta SIC_{DJF,NS}$ and Figure 12b shows, for each model, the percentage of sea ice cover change associated with each term in the regression model. According to the model of Eq. (1), the summer sea ice anomalies and AMOC strength anomalies have comparable effects on $\Delta SIC_{DJF,NS}$, with the AMOC playing a particularly important role in CNRM-CM5 and GISS-E2-R.

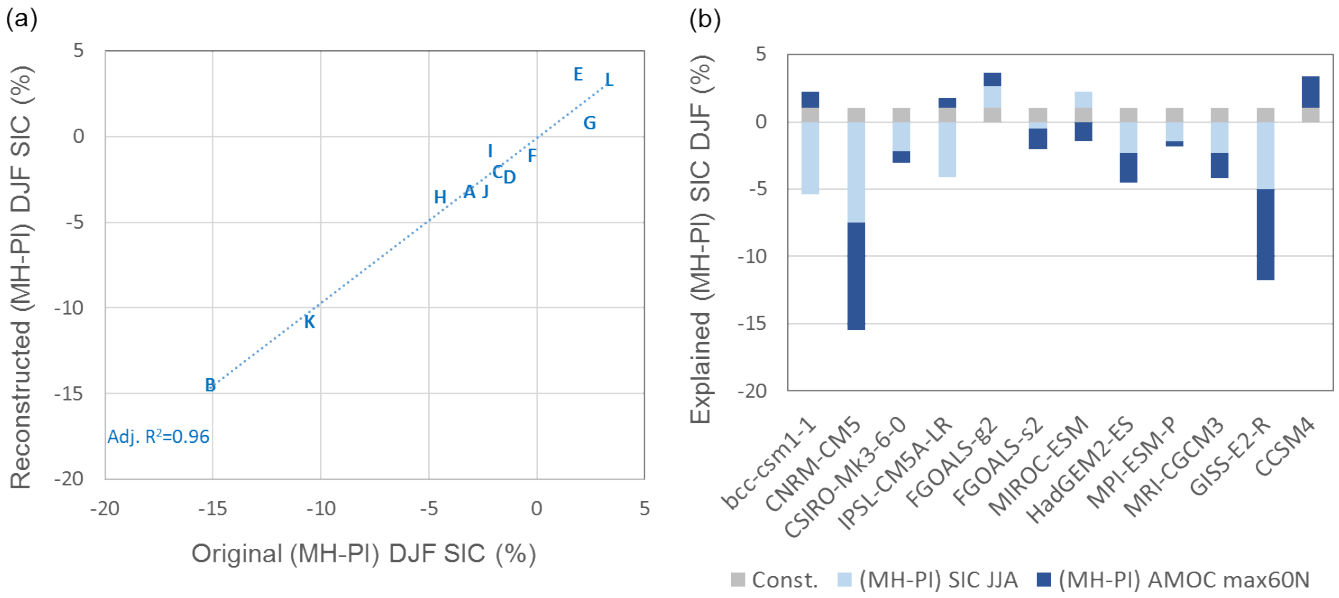

Figure12. Results of the multiple linear regression of $\Delta SIC_{DJF,NS}$ onto the MH anomaly of the AMOC maximum at 60°N and $\Delta SIC_{JJA,NS}$: (a) correspondence of the reconstructed and original $\Delta SIC_{DJF,NS}$; (b) winter sea ice cover anomaly associated to each model predictor, for the 12 models analyzed.

The adjusted r^2 can be mildly improved (to a value of 0.97) by adding the pre-industrial sea ice cover over the Nordic Seas region, $SIC_{DJF,PI,\ NS}$, as an extra predictor. However, the associated p value is 0.015, indicating a 1.5% chance that this predictor has in fact no effect on $\Delta SIC_{DJF,NS}$. Furthermore, the coefficient for this extra term is positive in this regression model (indicating

450 that climate models where more winter sea ice is present in the Nordic Seas region in pre-
451 industrial simulations tend to have positive or less negative Mid-Holocene winter sea ice
452 anomalies) but is negative in all other variable combinations analyzed. The role, if any, of the
453 background sea ice cover on the $SIC_{DJF, NS}$ anomalies thus remains uncertain.

454 The main caveat of the model in Eq (1) is that the two predictor variables are not independent.
455 $\Delta AMOC_{max,60°N}$ and $\Delta SIC_{JJA,NS}$ are correlated with an r^2 of 0.34, significant at the 95% level. It
456 is indeed very likely that the AMOC anomaly affects winter sea ice both directly, through
457 oceanic heat transport in winter, and indirectly, by influencing sea ice anomalies during summer
458 which, in turn, through ocean-sea ice-atmosphere feedbacks, can have a lasting effect on the
459 winter anomalies. Nevertheless, the AMOC may be affecting the annual sea ice anomalies and,
460 since sea ice seasonality is model-dependent, adding the summer sea ice as a second predictor
461 improves the results of the regression analysis. Such a regression could thus allow to explain
462 some of the spread that can be explained by local sea ice feedback and not only the AMOC
463 changes.

464 Summer sea ice cover anomalies are actually not entirely determined by the AMOC differences.
465 As shown in Figure 9, the Mid-Holocene experiences an important positive summer radiative
466 forcing in the high latitudes and the sensitivity of each model to this forcing is very likely to
467 have a strong effect on the summer sea ice anomalies. Since Mid-Holocene forcing is seasonal
468 and unevenly distributed over the globe, classical definitions of climate sensitivity do not apply
469 and could not be used to directly evaluate the model sensitivity effect on $\Delta SIC_{JJA,NS}$ and thus
470 on $\Delta SIC_{DJF,NS}$. We have attempted to use different first-order proxies of this effect that would
471 be less correlated with the AMOC change (such as summer SAT or surface downward
472 shortwave radiation anomalies over large domains in the Northern Hemisphere) as a
473 replacement for $\Delta SIC_{JJA,NS}$ in the regression model above, but with unsatisfactory results in
474 terms of p values and correlation coefficients.

Discussion and conclusions

We have analyzed Mid-Holocene winter anomalies over the North Atlantic sector in 12 PMIP3 models with the purpose of comparing the simulated European winter temperature anomalies with reconstructed data, and shedding light on their drivers.

Comparing the simulated winter near-surface air temperature anomalies with the recent pollen-based reconstruction of Mauri et al. (2014) for the Mid-Holocene, we found some qualitative agreement with the paleo-reconstruction for a few models, with pattern correlation coefficients above 0.6 for 5 out of the 12 models, mostly reflecting a north-south temperature anomaly gradient over Europe. All models underestimate the amplitude of the winter anomalies, however, as well as the amplitude of this meridional gradient, compared to the Mauri et al. (2014) reconstruction. Nevertheless, the uncertainties of this reconstruction do allow for a weaker gradient as found in the models, so that there is no striking inconsistency between this reconstruction and the models response to the Mid-Holocene forcing.

We have first analyzed the simulated large-scale atmospheric circulation anomalies over the North Atlantic sector. Our analysis has revealed a consistent climatological winter atmospheric response in Mid-Holocene consisting of two elements common to all models, though varying in spatial extent and intensity. The first is a dynamically forced anti-cyclonic anomaly over the south-western part of the North Atlantic, with a strong barotropic component. This structure is associated with a local weakening of the jet stream and a more pronounced separation between the eddy-driven and subtropical jet streams over the North Atlantic sector. The second element is a positive sea-level pressure anomaly over northern Africa with a shallow baroclinic structure. This SLP anomaly is a result of the colder atmospheric temperature in response to the strong negative radiative forcing at low latitudes, the effects of which are amplified over continental regions. In the same way, a shallow low-pressure anomaly is found in the north of

499 the basin, in thermal balance with positive temperature anomalies. For some models these SLP
500 anomalies could be interpreted as a NAO^+ signal, although the vertical structure of the NAO is
501 much more barotropic.

502 While some models exhibit a NAO^+-like atmospheric circulation anomaly near the surface in
503 winter, the ensemble of 12 PMIP3 models does not support a link between this type of large-
504 scale atmospheric response and the MH temperature anomaly patterns over Europe. Instead,
505 the simulated MH European winter temperature anomaly patterns are, in most models,
506 determined by the radiatively forced cold anomalies at low latitudes and the more model-
507 dependent sea ice anomalies over the Nordic Seas, with the latter responsible for approximately
508 three times more inter-model variability than the former.

509 The analyses carried out to understand the differences in these sea ice anomalies between the
510 models have revealed multiple footprints of the ΔSIC feedbacks onto other fields often
511 dominating the climatological anomalies in the Nordic Seas region. We have shown here the
512 signature of these feedbacks on the near-surface air temperature, but similar signatures have
513 also been found (not shown) on other variables. A very tight collocation between strong
514 negative (positive) sea ice anomalies and negative (positive) near-surface horizontal wind
515 divergence anomalies was found in all models for which the latter could be calculated, likely
516 explained by a response of the near-surface atmospheric circulation to the sea ice anomalies
517 and to the associated air-sea flux anomalies. A local increase in cloud cover over negative ΔSIC
518 regions (and *vice-versa*) has been found in most models, engendering marked local anomalies
519 of the downward longwave and shortwave radiative fluxes at the surface (positive and negative
520 respectively over regions of sea ice loss and vice-versa). A strong ΔSIC feedback has also been
521 found on the surface sensible heat flux (SH). In 3 out 12 models this corresponds to a simple
522 positive response of SH to a positive ΔSIC or vice-versa. In most models, however, the response
523 is more complex, taking the form of a strong positive-negative SH dipole over the ΔSIC region

524 depending on the background sea ice cover, which shows a subtle interplay of sea surface
525 temperature and air temperature anomalies in these regions.

526 These ubiquitous sea ice feedback signatures confirm the importance of a correct sea ice
527 representation in the models for representing the regional climate over Europe. All but three
528 models show a reduced winter sea ice cover in the Nordic Seas region in Mid-Holocene
529 compared to the pre-industrial climate. While not allowing for a quantitative model evaluation
530 of the sea-ice cover anomaly, a recent compilation of multi-proxy reconstructions of Mid-
531 Holocene ΔSIC which expands on the data set used in Klein et al. (2014) (Seidenkrantz, 2015,
532 personal communication) qualitatively confirms this result. We can thus conclude that the
533 models simulating an increase in NS winter sea ice cover in the Mid-Holocene, namely
534 FGOALS-g2, MIROC-ESM and CCSM4, are unrealistic for the Mid-Holocene climate in the
535 North Atlantic sector.

536 Sea ice feedback signatures dominating the climatological winter anomalies hinder the quest
537 for the causes of SIC anomalies in the model results. Nevertheless, we were able to highlight a
538 robust multi-model relationship between the MH winter SIC anomalies in the Nordic Seas
539 region and the anomalies in the Atlantic meridional overturning circulation, which points to the
540 AMOC as an important driver of the MH response of European winter temperatures.

541 The MH-PI differences in the atmospheric heat transport due to transient eddies form an
542 important potential source of information on the drivers of the SIC anomalies. However, these
543 differences could not be evaluated due to the lack of availability of the corresponding fields in
544 the PMIP3 data base. This type of drawback will be solved thanks to the inclusion of such fields
545 in the outputs from future model intercomparison exercises such as the upcoming CMIP6 and
546 PMIP4.

547 Another potential key player neglected here is the feedback from vegetation changes in the high
548 latitudes, which could also amplify the pattern found in the MH simulations (Wohlfahrt et al.
549 2008), potentially bringing the model simulations closer to MH observations.

550 We also know that PMIP3 models systematically underestimate the monsoon anomalies in the
551 Mid-Holocene (the "Green Sahara" event, Claussen & Gayler 1997). It is plausible that this
552 event was linked to a northward shift of the Hadley Cell (Claussen and Gayler 1997), which
553 would therefore not be captured or at best be severely underestimated by the models. We
554 conjecture that all models underestimate large-scale anomalies in the atmospheric circulation
555 that may have taken place (Gaetani et al. 2017) and may have affected temperature patterns
556 over Europe during MH winters. Our study, however, highlights the potential relevance of other
557 effects, which deserve further study.

558 While previous, paleo-reconstruction-based studies, often attribute Mid-Holocene winter
559 European temperature anomalies to a NAO^{+}-like atmospheric circulation anomaly, our analysis
560 of PMIP3 models suggests the possibility of an additional or even alternative explanation
561 coming from a larger geographical context. In this new view, based on the most skillful PMIP3
562 models, European winter temperature anomaly patterns are determined, to the south, by strong
563 low-latitude temperature responses to the seasonal negative radiative forcing and to the north
564 by feedbacks of the negative sea ice anomalies over the Nordic Seas on the atmosphere. Model
565 simulations also suggest that a major driving force for these sea ice anomalies is an
566 intensification of the Atlantic meridional overturning circulation in the Mid-Holocene
567 compared to the modern period, as indirectly suspected in Masson et al. (1999). This is in
568 agreement with reconstructions based on sortable silt in the North Atlantic, a proxy of deep
569 water circulation, which indicate a stronger deep current during the MH (Kissel et al. 2013).
570 The amplitude of the north-south gradient over Europe is weaker in the models than in the
571 reconstruction. We can suggest that this is related to a general bias of climate models in

representing the strong air-sea interaction as recently highlighted by the so-called signal to noise paradox by Scaife et al. (2018).

The cause for the changes in the AMOC has not been analyzed in the present paper since it necessitates a dedicated study. As noticed before, this could be related to a decrease in sea ice transport through Fram straight due to a lower sea ice production when insolation is larger in summer (Born et al. 2010). Another interesting factor could be related to the influence of the atmospheric circulation on the AMOC. For instance, variability of the AMOC over the last 60 years has been often related to NAO variations (Delworth et al. 2016; Swingedouw et al. 2015a). The mechanism is related to a cooling of the surface Labrador Sea during NAO^+ phases, which increases the Labrador deep water formation and a few years later the AMOC (Eden and Willebrand 2001). Thus, if the atmospheric circulation during the MH changed towards a NAO^+-like configuration, then it likely amplified the AMOC, as highlighted in Shi and Lohman (2016) for the ECHAM-FESOM-MPIOM climate model. In our present PMIP3 ensemble, the NAO changes are not the sole driver, since the relationship between our indices of NAO and AMOC changes are not significantly correlated (not shown).

If this interpretation is correct, it appears that the MH European winter temperatures can be both a testbed to estimate possible changes of the NAO and the AMOC in the near future. Since, as we find here, the inter-model differences in MH temperature anomalies are mainly explained by AMOC changes, we conclude that the MH is indeed an interesting case study to evaluate the sensitivity of the simulated AMOC to changes in radiative forcing. Nevertheless, to produce a correct assessment of models, we need to have a finer, quantitative AMOC reconstruction for this period. The use of a methodology combining climate models and available observational datasets, as employed for the deglaciation by Ritz et al. (2013) for instance, is an interesting approach to be developed. This may help to better decipher the sensitivity of the AMOC to

596 different forcings, which may provide new leads to reduce the very large uncertainty (Weaver
597 et al. 2012) concerning the future of the AMOC.

598 Acknowledgements

599 We wish to thank Marrit-Solveig Seidenkrantz, Hugues Goosse and Frédéric Hourdin for
600 fruitful discussions that have benefitted our study. This project would not have been possible
601 without the availability of PMIP3 data in a centralized, consistent format, for which we are
602 deeply thankful to the climate modeling centers listed in Table 1, to the groups behind the
603 ESGF portal, and in particular to Guillaume Levavasseur and Jean-Yves Peterschmitt, as well
604 as the FileFinderAR5 developed by Patrick Brockmann. To analyze the PMIP3 data, this
605 study benefited from the IPSL Prodiguer-Ciclad facility supported by CNRS, UPMC, Labex
606 L-IPSL which is funded by the ANR (Grant #ANR-10-LABX-0018) and by the European
607 FP7 IS-ENES2 project (Grant #312979). AGB was supported by the Swedish Research
608 Council Grant No. C0629701 (MILEX). The research leading to this study also received
609 funding from the French National Research Agency HAMOC project (Grant ANR-13-BS06-
610 0003).

611 References

612 Årthun, M. et al. (2017) Skillful prediction of northern climate provided by the ocean. Nat.
613 Commun. 8, 15875 doi: 10.1038/ncomms15875.

614 Bakker, P., and Coauthors, 2016: Fate of the Atlantic Meridional Overturning Circulation –
615 Strong decline under continued warming and Greenland melting. *Geophys. Res. Lett.*, 1–
616 9, doi:10.1002/2016GL070457.
617 http://onlinelibrary.wiley.com/doi/10.1002/2016GL070457/abstract.

618 Bao, Q., and Coauthors, 2013: The Flexible Global Ocean-Atmosphere-Land system model,
619 Spectral Version 2: FGOALS-s2. *Adv. Atmos. Sci.*, **30**, 561–576, doi:10.1007/s00376-

012-2113-9.

Berger, M., J. Brandefelt, and J. Nilsson, 2013: The sensitivity of the Arctic sea ice to orbitally induced insolation changes: A study of the mid-holocene paleoclimate modeling intercomparison project 2 and 3 simulations. *Clim. Past*, **9**, 969–982, doi:10.5194/cp-9-969-2013.

Boning, C. W., F. O. Bryan, W. R. Holland, and R. Doscher, 1995: Deep water formation and meridional overturning in a high-resolution model ofthe North Atlantic. *J. Phys. Oceanogr.*, **26**, 1142–1164.

Born, A., K. H. Nisancioglu, and P. Braconnot, 2010: Sea ice induced changes in ocean circulation during the Eemian. *Clim. Dyn.*, **35**, 1361–1371, doi:10.1007/s00382-009-0709-2.

Born, J. Mignot and T.F. Stocker (2015) Multiple Equilibria as a Possible Mechanism for Decadal Variability in the North Atlantic Ocean. *Journal of Climate* **28**, 8907-8922

Braconnot, P., S. P. Harrison, M. Kageyama, P. J. Bartlein, V. Masson-Delmotte, A. Abe-Ouchi, B. Otto-Bliesner, and Y. Zhao, 2012: Evaluation of climate models using palaeoclimatic data. *Nat. Clim. Chang.*, **2**, 417–424, doi:10.1038/nclimate1456. http://dx.doi.org/10.1038/nclimate1456.

Brewer, S., Guiot, J., and Torre, F.: Mid-Holocene climate change in Europe: a data-model comparison, Clim. Past, 3, 499-512, https://doi.org/10.5194/cp-3-499-2007, 2007.

Cattiaux, J., and C. Cassou, 2013: Opposite CMIP3/CMIP5 trends in the wintertime Northern Annular Mode explained by combined local sea ice and remote tropical influences. *Geophys. Res. Lett.*, **40**, 3682–3687, doi:10.1002/grl.50643.

Chabaud, L., M. F. Sanchez Goni, S. Desprat, and L. Rossignol, 2014: Land-sea climatic variability in the eastern North Atlantic subtropical region over the last 14,200 years:

644 Atmospheric and oceanic processes at different timescales. *The Holocene*, **24**, 787–797,
645 doi:10.1177/0959683614530439.

646 Claussen, M., and V. Gayler, 1997: The Greening of the Sahara during the Mid-Holocene:
647 Results of an Interactive Atmosphere-Biome Model. *Glob. Ecol. Biogeogr. Lett.*, **6**, 369–
648 377.

649 Collins, W. J., N. Bellouin, N. Gedney, P. Halloran, T. Hinton, J. Hughes, and C. D. Jones,
650 2011: Model Development Development and evaluation of an Earth-System model –
651 HadGEM2. 1051–1075, doi:10.5194/gmd-4-1051-2011.

652 Conil, S., and L. Z.-X. Li, 2005: Linearity of the Atmospheric Response to \textsc{N}orth
653 \textsc{A}tlantic SST and Sea Ice Anomalies. *J.\ Clim.*, **18**, 1986–2003.
654 http://dx.doi.org/10.1175/JCLI3388.1.

655 Davis, B. A. S., and S. Brewer, 2009: Orbital forcing and role of the latitudinal
656 insolation/temperature gradient. *Clim. Dyn.*, **32**, 143–165, doi:10.1007/s00382-008-
657 0480-9.

658 Delworth, T. L., F. Zeng, G. A. Vecchi, X. Yang, L. Zhang, and R. Zhang, 2016: The North
659 Atlantic Oscillation as a driver of rapid climate change in the Northern Hemisphere. *Nat.*
660 *Geosci.*, **9**, 509–512, doi:10.1038/ngeo2738.

661 Deser, C., R. Knutti, S. Solomon, and A. S. Phillips, 2012: Communication of the role of
662 natural variability in future North American climate. *Nat. Clim. Chang.*, **2**, 775–779,
663 doi:10.1038/nclimate1562. http://dx.doi.org/10.1038/nclimate1562.

664 Dufresne, J. L., and Coauthors, 2013: *Climate change projections using the IPSL-CM5 Earth*
665 *System Model: From CMIP3 to CMIP5*. 2123-2165 pp.

666 Eden, C., and J. Willebrand, 2001: Mechanisms of interannual to decadal variability of the
667 North Atlantic circulation. *J. Clim.*, **14**, 2266–2280, doi:10.1175/1520-

668 0442(2001)014<2266:MOITDV>2.0.CO;2.

669 Escudier, R., J. Mignot, and D. Swingedouw, 2013: A 20-year coupled ocean-sea ice-
670 atmosphere variability mode in the North Atlantic in an AOGCM. *Clim. Dyn.*, **40**, 619–
671 636.

672 Fischer, N., and J. H. Jungclaus, 2011: Evolution of the seasonal temperature cycle in a
673 transient Holocene simulation: Orbital forcing and sea-ice. *Clim. Past*, **7**, 1139–1148,
674 doi:10.5194/cp-7-1139-2011.

675 Fischer et al. (2018) Palaeoclimate constraints on the impact of 2 °C anthropogenic warming
676 and beyond. Nat. Geosc. 1, 474-485.

677 Gaetani M., Messori G., Zhang Q., Flamant C., Pausata F. S. R. (2017) Understanding the
678 mechanisms behind the northward extension of the West African Monsoon during the
679 Mid-Holocene. *Journal of Climate*, American Meteorological Society, 2017, 30 (19),
680 pp.7621-7642.

681 Gent, P. R., and Coauthors, 2011: The community climate system model version 4. *J. Clim.*,
682 **24**, 4973–4991, doi:10.1175/2011JCLI4083.1.

683 Gladstone, R. M., and Coauthors, 2005: Mid-Holocene NAO: A PMIP2 model
684 intercomparison. *Geophys. Res. Lett.*, **32**, 1–4, doi:10.1029/2005GL023596.

685 Goosse, H., F. Selten, R. Haarsma, and J. Opsteegh, 2002: A mechanism of decadal
686 variability of the sea-ice volume in the Northern Hemisphere. *Clim. Dyn.*, **19**, 61–83,
687 doi:10.1007/s00382-001-0209-5.

688 Guyard, H., E. Chapron, G. St-Onge, and J. Labrie, 2013: Late-Holocene NAO and oceanic
689 forcing on high-altitude proglacial sedimentation (Lake Bramant, Western French Alps).
690 *The Holocene*, **23**, 1163–1172, doi:10.1177/0959683613483616.
691 http://hol.sagepub.com/content/23/8/1163.abstract.

692 Haarsma, R. J., F. M. Selten and S. S. Drijfhout (2015) Decelerating Atlantic meridional
693 overturning circulation main cause of future west European summer atmospheric
694 circulation changes. *Environmental Research Letters*, **10** (9), doi:10.1088/1748-
695 9326/10/9/094007.

696 Harrison, S. P., P. J. Bartlein, K. Izumi, G. Li, J. Annan, J. Hargreaves, P. Braconnot, and M.
697 Kageyama, 2015: Evaluation of CMIP5 palaeo-simulations to improve climate
698 projections. *Nat. Clim. Chang.*, **5**, 735–743, doi:10.1038/nclimate2649.
699 http://www.nature.com/doifinder/10.1038/nclimate2649.

700 Hawkins, E., and R. Sutton, 2009: The potential to narrow uncertainty in regional climate
701 predictions. *Bull. Am. Meteorol. Soc.*, **90**, 1095–1107, doi:10.1175/2009BAMS2607.1.

702 Huck, T., A. De Colin Verdière, P. Estrade, and R. Schopp, 2008: Low-frequency variations
703 of the large-scale ocean circulation and heat transport in the North Atlantic from 1955-
704 1998 in situ temperature and salinity data. *Geophys. Res. Lett.*, **35**, 1–5,
705 doi:10.1029/2008GL035635.

706 Hurrell, J. W., 1995: Decadal Trends in the North Atlantic Oscillation : Regional
707 Temperatures and Precipitation. Science Vol. 269, No. 5224, pp. 676-679.

708 Hurrell, J. W., and C. Deser, 2010: North Atlantic climate variability: The role of the North
709 Atlantic Oscillation. *J. Mar. Syst.*, **79**, 231–244, doi:10.1016/j.jmarsys.2009.11.002.

710 IPCC Working Group 1, I., and Coauthors, 2013: IPCC, 2013: Climate Change 2013: The
711 Physical Science Basis. Contribution of Working Group I to the Fifth Assessment Report
712 of the Intergovernmental Panel on Climate Change. *IPCC*, **AR5**, 1535.

713 Jackson, L. C. et al. (2015) Global and European climate impacts of a slowdown of the
714 AMOC in a high resolution GCM. *Climate Dynamics*, **45** (11-12), 3299-3316,
715 doi:10.1007/s00382-015-2540-2.

716 Jungclaus, J. H., and Coauthors, 2013: Characteristics of the ocean simulations in the Max
717 Planck Institute Ocean Model (MPIOM) the ocean component of the MPI-Earth system
718 model. **5**, 422–446, doi:10.1002/jame.20023.

719 Kissel, C., A. Van Toer, C. Laj, E. Cortijo, and E. Michel, 2013: Variations in the strength of
720 the North Atlantic bottom water during Holocene. *Earth Planet. Sci. Lett.*, **369–370**,
721 248–259, doi:10.1016/j.epsl.2013.03.042. http://dx.doi.org/10.1016/j.epsl.2013.03.042.

722 Klein, F., H. Goosse, A. Mairesse, A. De Vernal, and P. L. Pasteur, 2014: Model – data
723 comparison and data assimilation of mid-Holocene Arctic sea ice concentration. 1145–
724 1163, doi:10.5194/cp-10-1145-2014.

725 Li, L., and Coauthors, 2013: The flexible global ocean-atmosphere-land system model, Grid-
726 point Version 2: FGOALS-g2. *Adv. Atmos. Sci.*, **30**, 543–560, doi:10.1007/s00376-012-
727 2140-6.

728 Masson, V., R. Cheddadi, P. Braconnot, S. Joussaume, and D. Texier, 1999: Mid-Holocene
729 climate in Europe: What can we infer from PMIP model-data comparisons? *Clim. Dyn.*,
730 **15**, 163–182, doi:10.1007/s003820050275.

731 Massonnet F., T. Fichefet, H. Goosse, C. M. Bitz, G. Philippon-Berthier, M. M. Holland, P. -
732 Y. Barriat (2012) Constraining projections of summer Arctic sea ice. *The Cryosphere* 6,
733 1383-1394.

734 Mauri, A., B. A. S. Davis, P. M. Collins, and J. O. Kaplan, 2014: The influence of
735 atmospheric circulation on the mid-Holocene climate of Europe: A data-model
736 comparison. *Clim. Past*, **10**, 1925–1938, doi:10.5194/cp-10-1925-2014.

737 McCarthy, G. D. et al., 2015: Measuring the Atlantic Meridional Overturning Circulation at
738 26 degrees N. *Progress in Oceanography*, **130**, 91-111,
739 doi:10.1016/j.pocean.2014.10.006.

740 Otto, J., T. Raddatz, and M. Claussen, 2009: Climate variability-induced uncertainty in mid-
741 Holocene atmosphere-ocean-vegetation feedbacks. *Geophys. Res. Lett.*, **36**, 1–5,
742 doi:10.1029/2009GL041457.

743 Ritz, S. P., T. F. Stocker, J. O. Grimalt, L. Menviel, and A. Timmermann, 2013: Estimated
744 strength of the Atlantic overturning circulation during the last deglaciation. *Nat. Geosci.*,
745 **6**, 208–212, doi:10.1038/ngeo1723. http://www.nature.com/doifinder/10.1038/ngeo1723.

746 Rotstayn, L. D., S. J. Jeffrey, M. A. Collier, S. M. Dravitzki, A. C. Hirst, J. I. Syktus, and K.
747 K. Wong, 2012: and Physics Aerosol- and greenhouse gas-induced changes in summer
748 rainfall and circulation in the Australasian region : a study using single-forcing climate
749 simulations. 6377–6404, doi:10.5194/acp-12-6377-2012.

750 Saint-Lu, M., P. Braconnot, J. Leloup, and O. Marti, 2016: The role of El Ni??o in the global
751 energy redistribution: a case study in the mid-Holocene. *Clim. Dyn.*, 1–18,
752 doi:10.1007/s00382-016-3266-5.

753 Scaife A., Smith, D. (2018) A signal-to-noise paradox in climate science. Climate and
754 Atmospheric Science 1:28 ; doi:10.1038/s41612-018-0038-4

755 Schmidt, G. A., and Coauthors, 2006: Present-Day Atmospheric Simulations Using GISS
756 ModelE: Comparison to In Situ, Satellite, and Reanalysis Data. *J. Clim.*, **19**, 153–192,
757 doi:10.1175/JCLI3612.1. http://journals.ametsoc.org/doi/abs/10.1175/JCLI3612.1.

758 Schmidt, G. A., and Coauthors, 2014: Using palaeo-climate comparisons to constrain future
759 projections in CMIP5. *Clim. Past*, **10**, 221–250, doi:10.5194/cp-10-221-2014.

760 Shi, X., and G. Lohmann (2016), Simulated response of the mid- Holocene Atlantic
761 meridional overturning circulation in ECHAM6-FESOM/MPIOM, J. Geophys. Res.
762 Oceans, 121, 6444–6469, doi:10.1002/ 2015JC011584.

763 Swingedouw, D., P. Braconnot, and O. Marti, 2006: Sensitivity of the Atlantic Meridional

764 Overturning Circulation to the melting from northern glaciers in climate change
765 experiments. *Geophys. Res. Lett.*, **33**.

766 ——, J. Mignot, P. Braconnot, E. Mosquet, M. Kageyama, and R. Alkama, 2009: Impact of
767 freshwater release in the north atlantic under different climate conditions in an OAGCM.
768 *J. Clim.*, **22**, 6377–6403, doi:10.1175/2009JCLI3028.1.

769 Swingedouw, D., and Coauthors, 2015a: Bidecadal North Atlantic ocean circulation
770 variability controlled by timing of volcanic eruptions. *Nat. Commun.*, **in press**.

771 Swingedouw, D., C. B. Rodehacke, S. M. Olsen, M. Menary, Y. Gao, U. Mikolajewicz, and J.
772 Mignot, 2015b: On the reduced sensitivity of the Atlantic overturning to Greenland ice
773 sheet melting in projections: a multi-model assessment. *Clim. Dyn.*, **44**, 3261–3279,
774 doi:10.1007/s00382-014-2270-x. http://dx.doi.org/10.1007/s00382-014-2270-x.

775 Voldoire, A., and Coauthors, 2013: The CNRM-CM5.1 global climate model: Description
776 and basic evaluation. *Clim. Dyn.*, **40**, 2091–2121, doi:10.1007/s00382-011-1259-y.

777 Watanabe, M., M. Chikira, Y. Imada, and M. Kimoto, 2011: Convective control of ENSO
778 simulated in MIROC. *J. Clim.*, **24**, 543–562, doi:10.1175/2010JCLI3878.1.

779 Weaver, A. J., and Coauthors, 2012: Stability of the Atlantic meridional overturning
780 circulation: A model intercomparison. *Geophys. Res. Lett.*, **39**, 1–7,
781 doi:10.1029/2012GL053763.

782 Wohlfahrt, J., S. P. Harrison, P. Braconnot, C. D. Hewitt, A. Kitoh, U. Mikolajewicz, B. L.
783 Otto-Bliesner, and S. L. Weber, 2008: Evaluation of coupled ocean-atmosphere
784 simulations of the mid-Holocene using palaeovegetation data from the northern
785 hemisphere extratropics. *Clim. Dyn.*, **31**, 871–890, doi:10.1007/s00382-008-0415-5.

786 Xin, X., L. Zhang, J. Zhang, T. Wu, and Y. Fang, 2013: Climate Change Projections over
787 East Asia with BCC _ CSM1 . 1 Climate Model under RCP Scenarios. **91**, 413–429,

788 doi:10.2151/jmsj.2013-401.

789 Yukimoto, S., Y. Adachi, M. Hosaka, and T. Sakami, 2012: A New Global Climate Model of
790 the Meteorological Research Institute : MRI-CGCM3 — Model Description and Basic
791 Performance —. **90**, doi:10.2151/jmsj.2012-A02.